Accuracy of expressions for the fill factor of a solar cell in terms of open-circuit voltage and ideality factor

Mehdi Leilaeioun and Zachary C. Holman
School of Electrical, Computer, and Energy Engineering, Arizona State University, Tempe, Arizona 85287-5706, USA

(Received 12 April 2016; accepted 29 August 2016; published online 30 September 2016)

An approximate expression proposed by Green predicts the maximum obtainable fill factor (*FF*) of a solar cell from its open-circuit voltage (V_{oc}). The expression was originally suggested for silicon solar cells that behave according to a single-diode model and, in addition to V_{oc}, it requires an ideality factor as input. It is now commonly applied to silicon cells by assuming a unity ideality factor—even when the cells are not in low injection—as well as to non-silicon cells. Here, we evaluate the accuracy of the expression in several cases. In particular, we calculate the recombination-limited *FF* and V_{oc} of hypothetical silicon solar cells from simulated lifetime curves, and compare the exact *FF* to that obtained with the approximate expression using assumed ideality factors. Considering cells with a variety of recombination mechanisms, wafer doping densities, and photogenerated current densities reveals the range of conditions under which the approximate expression can safely be used. We find that the expression is unable to predict *FF* generally: For a typical silicon solar cell under one-sun illumination, the error is approximately 6% absolute with an assumed ideality factor of 1. Use of the expression should thus be restricted to cells under very low or very high injection. *Published by AIP Publishing.* [http://dx.doi.org/10.1063/1.4962511]

I. INTRODUCTION

The fill factor (*FF*) of a solar cell is sensitive to nearly every processing step during cell fabrication and therefore tends to fluctuate across a batch and between batches of solar cells more than open-circuit voltage (V_{oc}) or short-circuit current density (J_{sc}). For silicon solar cells, it is now common to calculate the fill factor in the absence of external series resistance (the so-called pseudo fill factor, *pFF*) from Suns-V_{oc} measurements,[1] and to use this value as an upper limit against which the oft-varying actual *FF* can be compared.[2] Prior to the introduction of the Suns-V_{oc} technique, an approximate expression was suggested by Green[3] to predict the *pFF* from the V_{oc} of a silicon solar cell. (The fill factor calculated by these expressions is in fact that with no series resistance *and* with infinite shunt resistance, which is not true of *pFF*, but low shunt resistance is not normally a problem in silicon solar cells.) This expression is convenient because it allows one to, e.g., calculate the *pFF* of a cell reported in the literature without Suns-V_{oc} data or to use the implied open-circuit voltage (iV_{oc}) to gain insight into *FF* at early stages of cell processing (e.g., after passivation).[1,2,4] However, the expression was proposed to explain the behavior of cells operating in low injection, for which the recombination rate is linear in excess carrier density. The expression can be extended to higher injection by including a non-unity ideality factor. However, the formula accepts a *single* ideality factor as input, and, as ideality factor varies with injection level and is determined by the dominant recombination mechanism,[5] it is not obvious which ideality factor to use.

In recent years, this expression has often been used to calculate *FF* without regard for the aforementioned limitations. In particular, it has been applied for silicon cells under mid and high injections and even for *non-silicon* solar cells including polymer, organic, dye-sensitized, and multi-junction concentrator cells.[5–15] In some cases, this has led to misleading predictions—often overpredictions—of efficiency limits. In addition, an ideality factor of 1 is most frequently supposed, regardless of the injection level and dominant recombination process(es).

In this paper, we investigate the accuracy of the *FF* approximation to understand the range of conditions for which it can safely be used. Our approach is to consider hypothetical solar cells with known recombination, from which we can calculate the effective lifetime of minority carriers. From the lifetime curves, we calculate the corresponding exact iV_{oc} and *iFF*, and compare the latter to the *FF* computed with the approximate expression using the exact iV_{oc}. (Note that, hereafter, iV_{oc} and *iFF* are referred to simply as V_{oc} and *FF* since they are identical in our study of hypothetical, recombination-limited cells with no series resistance and infinite shunt resistance.) We find that the deviations are significant whenever the incorrect ideality factor is assumed, and non-negligible even with the "correct" ideality factor. Particular attention is thus required when using the expression. Along the way, we elucidate the dependence of V_{oc} and *FF* on recombination mechanism, wafer doping density, and illumination.

II. MODELING

A. Calculation approach

For simplicity, we limit our analysis to solar cells on n-type silicon wafers, though it can be easily extended to p-type wafers. Figure 1 shows the calculation approach employed in this paper. We begin by generating lifetime data for hypothetical silicon solar cells using recent models for intrinsic (radiative and Auger)[16] and bulk defect (Shockley-

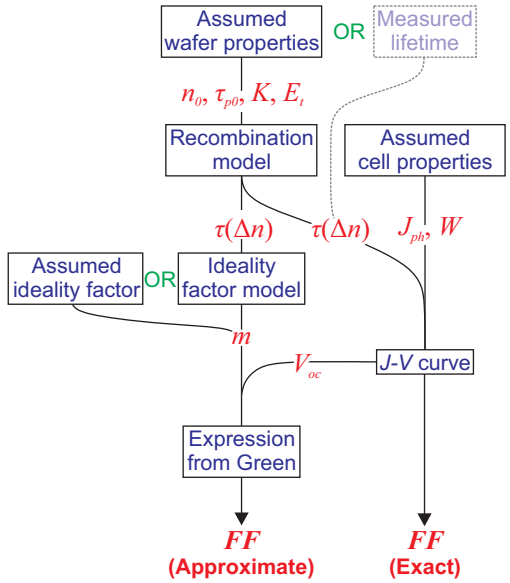

FIG. 1. Illustration of the calculation approach used to find both the exact and approximate *FF* of a given hypothetical solar cell. Note that, though not done in this paper, measured lifetimes (dashed box) may be substituted for calculated lifetimes.

Read-Hall, SRH) recombination.[17,18] We neglect surface recombination and assume perfect passivation for simplicity; we find intrinsic and SRH recombination to be sufficient to evaluate the accuracy of the approximate *FF* expressions. Next, using the detailed balance model of Richter *et al.*,[19] we compute current density-voltage (*J-V*) characteristics from the lifetime data and find the exact *FF* and V_{oc} values for each hypothetical cell. We also extract the injection-dependent ideality factor from the lifetime using an expression developed by Hameiri *et al.*[5] In select cases, the ideality factor of a cell at open circuit or at maximum power is then inserted, along with the exact V_{oc} of that cell, into the expression proposed by Green to find the corresponding approximate *FF*. In other cases, the injection dependence of the ideality factor is ignored and a value of 0.7, 1, or 2 is assumed. Finally, we compare the approximate and exact *FF* values and calculate the relative difference between them.

B. Lifetime curves

1. Intrinsic recombination model

We used the parameterization recently published by Richter *et al.* to model intrinsic recombination in silicon solar cells.[16] The model outputs minority-carrier intrinsic lifetime as a function of excess carrier density. The main advantage of this model over previous models is that it considers the increased Auger recombination probability caused by Coulomb interactions of electrons and holes. Radiative recombination within the Richter parameterization is based on the radiative coefficients measured by Trupke *et al.*,[20] and—as with Auger recombination—the effect of Coulomb interactions is included using the model introduced by Altermatt *et al.*[21] The parameterization also considers the influence of bandgap narrowing on the effective intrinsic carrier density, which increases with doping and injection level.[22,23]

According to the Richter model, the minority-carrier intrinsic lifetime in silicon is given by

$$\tau_{intr}=\frac{\Delta n}{\left(np-n_{i,eff}^2\right)\left(\begin{matrix}2.5\times10^{-31}g_{eeh}(n_0)+8.5\times10^{-32}g_{ehh}(p_0)\\+3.0\times10^{-29}\Delta n^{0.92+B_{rel}B_{low}}\end{matrix}\right)} \tag{1}$$

with Coulomb interaction enhancement factors

$$g_{eeh}(n_0)=1+13\left\{1-\tanh\left[\left(\frac{n_0}{N_{0,eeh}}\right)^{0.66}\right]\right\}$$
$$g_{ehh}(p_0)=1+7.5\left\{1-\tanh\left[\left(\frac{p_0}{N_{0,ehh}}\right)^{0.63}\right]\right\}. \tag{2}$$

In these equations, n and p are the electron and hole densities, n_0 and p_0 are the equilibrium electron and hole densities, Δn is the excess carrier density, $n_{i,eff}$ is the effective intrinsic carrier density obtained using the empirical expression of Ref. 23 that considers bandgap narrowing as a function of dopant concentration, $B_{low}=4.73\times10^{-15}\,\mathrm{cm^3\,s^{-1}}$ is the radiative recombination coefficient for lightly doped silicon in low injection,[20] B_{rel} is the relative radiative recombination coefficient according to Ref. 21, and $N_{0,eeh}=3.3\times10^{17}\mathrm{cm^{-3}}$ and $N_{0,ehh}=7\times10^{17}\mathrm{cm^{-3}}$ are empirical constants.

2. Bulk-defect recombination model

A SRH model[17,18] was used for recombination through bulk defect states. SRH models consider a single trap level within the bandgap that has an assumed carrier capture behavior. The SRH model introduced by Rein *et al.*[24] gives the minority-carrier lifetime in n-type silicon as

$$\tau_{SRHn-type}=\tau_{p0}\left[\frac{n_0+p_1+\Delta n}{n_0+p_0+\Delta n}+K\frac{n_1+p_0+\Delta n}{n_0+p_0+\Delta n}\right]. \tag{3}$$

In Equation (3), τ_{p0} is the equilibrium capture time constant of holes, given by

$$\tau_{p0}=\frac{1}{\sigma_p v_{th}N_t}, \tag{4}$$

where σ_p is the capture cross section for holes, v_{th} is the thermal velocity, and N_t is the defect density. The symmetry factor, K, in Equation (3) is characteristic of a defect and defined by the ratio of the hole and electron capture cross sections: $K=\sigma_p/\sigma_n$. n_1 and p_1 are the SRH electron and hole densities, given by

$$n_1=N_C\exp\left(-\frac{E_C-E_t}{k_BT}\right),\quad p_1=N_V\exp\left(-\frac{E_t-E_V}{k_BT}\right), \tag{5}$$

where E_C and E_V are the energies of the conduction and the valence band edges, E_t is the energy of the trap, N_C and N_V are the effective densities of states in the conduction and the valence bands, and k_B and T have their usual meanings.

3. Effective lifetime

The effective lifetime τ_{eff} was obtained from the intrinsic and SRH lifetimes by adding them in parallel:

$$\frac{1}{\tau_{eff}} = \frac{1}{\tau_{\text{intr}}} + \frac{1}{\tau_{SRH}}. \tag{6}$$

C. *J-V* characteristics and exact *FF*

We used the approach suggested by Tiedje and Yablonovitch, and demonstrated recently by Kerr *et al.* and Richter *et al.*, to assess the limiting efficiency of silicon solar cells in the absence of parasitic optical and electrical losses.[19,25,26] This model assumes narrow-base conditions (the quasi-Fermi levels are constant within the base), for which the quasi-Fermi level separation is equal to the output voltage, given by[27,28]

$$\begin{aligned} V &= V_{jn} + V_{jp} = (\varphi_i - \varphi_n) + (\varphi_p - \varphi_i) \\ &= \frac{k_B T}{q} \ln\left((n_0 + \Delta n)(p_0 + \Delta n)/n_{i,eff}^2\right), \end{aligned} \tag{7}$$

where φ_i, φ_n, and φ_p are the intrinsic Fermi potential, electron quasi-Fermi potential, and hole quasi-Fermi potential, respectively. Note that the narrow-base assumption is not valid when the minority-carrier diffusion length is comparable to or smaller than the wafer thickness (e.g., for low-quality multicrystalline wafers with $\tau_{p0} < 50\,\mu$s), a situation not encountered in this study. The output current of the solar cell is given by the difference between the generation and recombination current densities

$$J = J_{ph} - qWR = J_{ph} - qW\Delta n/\tau_{eff}, \tag{8}$$

where J_{ph} is the photogenerated current density, q is the electronic charge, W is the cell thickness, and R is the total recombination rate. For a given value of Δn, Equations (7) and (8) yield the output voltage and current of the solar cell (after τ_{eff} is calculated with Equation (6)); sweeping Δn thus results in a J–V curve from which the FF can be determined.

D. Injection-dependent ideality factor

The approximate FF expressions require a single ideality factor m as input. Most often, a value is assumed or extracted from the J–V curve of a completed solar cell by fitting with a diode model. Here, in select instances, we used the formalism reported by Hameiri *et al.*[5] to calculate ideality factor from the minority-carrier effective lifetime (expressed as the recombination rate) as a function of the excess carrier density:

$$m = \left(\frac{1}{n} + \frac{1}{p}\right) R \frac{d\Delta n}{dR} = \frac{2\Delta n + n_0}{\Delta n(\Delta n + n_0)} R \frac{d\Delta n}{dR}. \tag{9}$$

E. Approximate *FF*

Green proposed an approximate empirical equation for FF in terms of V_{oc} for cases in which the ideality factor is known, the series resistance is zero, and the shunt resistance is infinite[3]:

$$FF = \frac{v_{oc} - \ln(v_{oc} + 0.72)}{v_{oc} + 1} \tag{10}$$

in which

$$v_{oc} = \frac{V_{oc}}{(mk_BT/q)}. \tag{11}$$

"Approximate FF" is hereafter used to refer to the FF values calculated with this expression.

Note that Swanson and Sinton derived a similar but less common expression for FF in terms V_{oc} from a different starting point.[27] These authors observed that, over a wide range of conditions, the power of a solar cell evaluated at 95% of its J_{sc} is uncannily similar to the maximum power of the cell. Consequently, in the particular case in which the recombination rate is proportional to excess carrier density, the excess carrier density at the maximum power point is 5% (a factor of 1/20) its value at open circuit ($\Delta n_{mpp} = 0.05\Delta n_{oc}$). The output current and voltage at maximum power are thus

$$J_{mpp} = 0.95 J_{sc}, \tag{12a}$$

$$V_{mpp} = V_{oc} - (mk_BT/q)\ln(20). \tag{12b}$$

Interestingly, Equation (12) indicates that V_{mpp} will always be 78 mV lower than V_{oc}, provided that the cell is in low injection ($m = 1$). Finally, FF can be calculated as

$$FF = \frac{V_{mpp}J_{mpp}}{V_{oc}J_{sc}} = \left(1 - \frac{1}{20}\right)\frac{v_{oc} - \ln(20)}{v_{oc}} \approx \frac{v_{oc} - \ln(20)}{v_{oc} + v_{oc}/20}. \tag{13}$$

Figure 2 compares the FF calculated with the expression from Swanson and Sinton to that calculated with the expression from Green for the commonly assumed ideality factors $m = 0.7$, 1, and 2. Despite their different origins and functional dependencies, the two expressions give very similar results, particularly for low injection ($m = 1$), and, thus any limitations encountered in our analysis of the expression from Green apply equally to the expression from Swanson and Sinton.

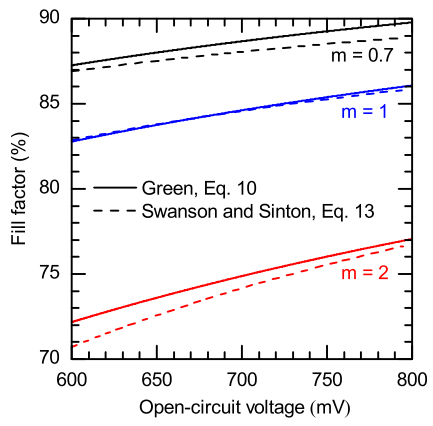

FIG. 2. FF values calculated with the approximate expressions from Green and Swanson and Sinton for a range of typical V_{oc}s and ideality factors.

III. RESULTS

In assessing Equation (10), we consider a hypothetical solar cell exhibiting only intrinsic recombination, only SRH bulk recombination, or both mechanisms simultaneously. The first two cases are illustrative because they have well-defined limiting ideality factors in high and low injection, whereas the third is representative of a real solar cell with a mediocre bulk lifetime but excellent surface passivation. (The third is likely also representative of a solar cell with excellent bulk lifetime but mediocre surface passivation—which we do not explicitly treat here—because surface recombination is also accurately modeled with an SRH formalism in most cases.) Figure 3 shows the V_{oc}s calculated for these three cases using the methodology described in Section II for a 170-μm-thick solar cell. The data are displayed as a contour plot in which the wafer doping density and photogenerated current density are varied. These quantities were chosen for the axes because doping density is the only variable parameter that influences the intrinsic lifetime (Equation (1)) and is one of the few parameters that an ingot manufacturer can easily control; the photogenerated current density appears in Equation (8) and changes the excess carrier density at open circuit and thus the corresponding V_{oc}. In practice, the photogenerated current density changes over the course of a day, when placing a cell under concentration, or when using a silicon cell in a tandem. It also varies with wafer thickness—which is a suitable alternative x-axis variable for Figure 3 if particular illumination conditions (e.g., AM1.5 G) are assumed[19]—though the two are treated independently in Equation (8). Doping density enters into the SRH lifetime (Equation (3)) in addition to the intrinsic lifetime, but so do several other parameters that characterize the assumed bulk defect. Throughout this paper, we assumed $\tau_{p0} = 500\ \mu$s, $K = 1$, and $E_t = 0.5$ eV (with $E_V = 0$). This hypothetical defect is representative of many real recombination-active defects in silicon (e.g., Mo, Cr, Ti, and Fe), which are near mid-gap and have near-unity capture cross section ratios.[29–33] In fact, the SRH lifetime changes little for 0.3 eV $< E_t <$ 0.8 eV and $0.2 < K < 5$. τ_{p0} was arbitrarily chosen based on measured lifetimes in, e.g., high-quality multicrystalline or low-quality Czochralski wafers.[34] As Equation (3) indicates, τ_{p0} simply scales the SRH lifetime.

The intrinsic-recombination-limited V_{oc} (Figure 3(a)) and the SRH-recombination-limited V_{oc} (Figure 3(b)) are both independent of doping density in high injection ($\Delta n > 10 n_0$), but they have opposite dependencies on doping in low injection ($\Delta n < 0.1 n_0$). We briefly digress to explore why. In open circuit, $J = 0$ and Equation (8) can be rearranged as

$$\Delta n = \frac{J_{ph}\tau_{eff}}{qW}. \tag{14}$$

Inserting this into Equation (7) and noting that p_0 is negligible in n-type wafers yields an expression for V_{oc} that can be further simplified in low injection to

$$V_{oc} = C_0\left(\ln\left(\frac{J_{ph}}{W}\right) + \ln(n_0) + \ln(\tau_{eff,oc})\right) + C_1 \tag{15a}$$

and in high injection to

$$V_{oc} = 2C_0\left(\ln\left(\frac{J_{ph}}{W}\right) + \ln(\tau_{eff,oc})\right) + C_2, \tag{15b}$$

where

$$C_0 = \frac{k_B T}{q}, \quad C_1 = -\frac{k_B T}{q}\ln\left(q n_{i,eff}^2\right),$$
$$C_2 = -\frac{k_B T}{q}\ln(q n_{i,eff}) \tag{15c}$$

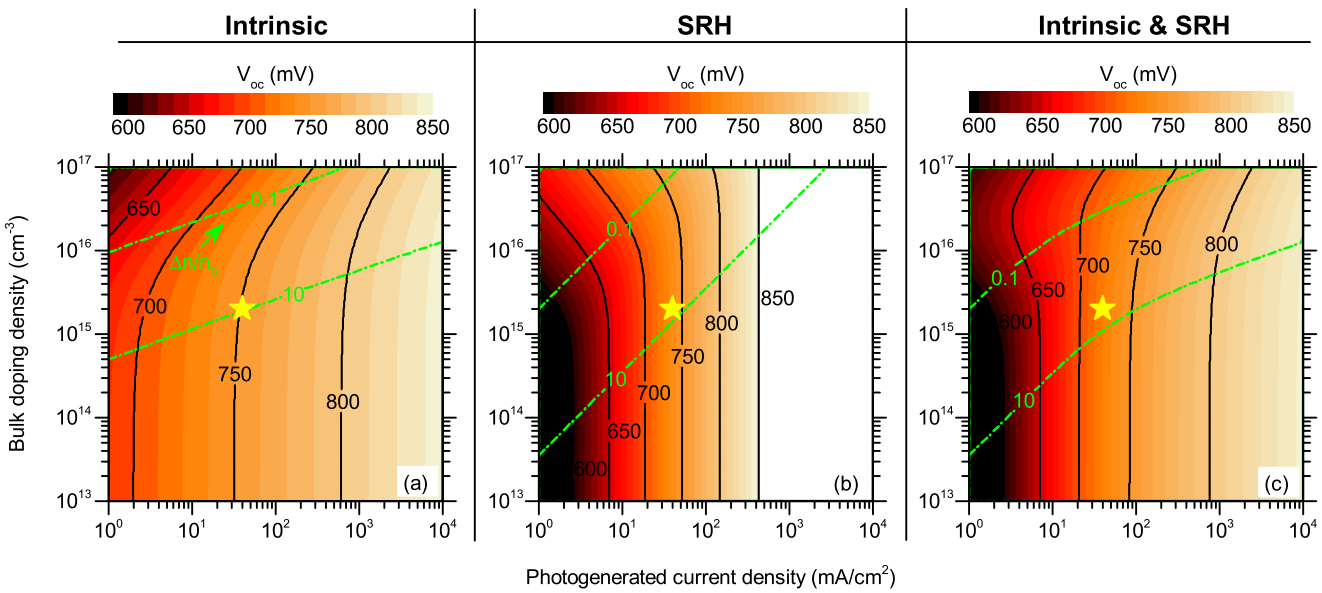

FIG. 3. Exact V_{oc}s of silicon solar cells on n-type, 170-μm-thick wafers with varying doping density under varying illumination levels (photogenerated current densities). V_{oc}s are shown for cells with intrinsic recombination, SRH recombination, and intrinsic and SRH recombination in (a), (b), and (c), respectively. The color scale is the same for each plot. The dash-dotted green lines denote doping densities and photogenerated current densities for which n/n_0 is 0.1 or 10; these values are used to denote the boundaries of low injection (region above the upper green line) and high injection (region below the lower green line). The yellow stars correspond to a typical solar cell with a 2 Ω cm n-type wafer under AM1.5G illumination.

are constants and $\tau_{eff,oc}$ is the effective lifetime at open circuit. We first consider SRH recombination (Figure 3(b)), which is the simpler of the two cases. Looking at Equation (3) and Figure 4(b), in high injection the effective lifetime is independent of photogenerated current density (or, specifically, Δn) and doping density ($\tau_{SRH} = \tau_{p0}\ (1+K) = 1$ ms), and, thus Equation (15b) indicates that V_{oc} scales with the logarithm of J_{ph} and is unaffected by n_o—hence the evenly spaced vertical contour lines in the lower right half of Figure 3(b). In low injection (upper left corner of Figure 3(b)), the lifetime is again independent of photogenerated current density and doping density ($\tau_{SRH} = \tau_{p0} = 0.5$ ms; see Figure 4(b)), but the extra term in Equation (15a) causes the V_{oc} to increase with the logarithm of n_o in addition to J_{ph}, hence the diagonal contour lines (evenly spaced along both the x- and y-axes).

For intrinsic recombination (Figure 3(a)), in high injection the effective lifetime falls with increasing J_{ph} (increasing Δn in Equation (1); see Figure 4(a)) but not as fast as J_{ph} itself increases (Equation (15b)). This again causes a logarithmic increase of V_{oc} with J_{ph} (C_1 is small), but with weaker dependence than for SRH recombination (evenly spaced vertical contour lines with wider spacing). In low injection, the lifetime is constant with respect to J_{ph} (Figure 4(a)) yet again giving a logarithmic increase of V_{oc} with J_{ph}. Unlike for SRH recombination, however, the low-injection lifetime decreases with increasing n_o and does so faster than n_o itself increases, so that V_{oc} *decreases* with increasing doping (see Equation (15a)). Interestingly, the trends in Figure 3(a), which display the injection-level dependence just described, are not directly determined by the recombination mechanism (radiative or Auger). In particular, Auger recombination dominates whenever the excess carrier density ($n = n_0 + \Delta n$) is large, which occurs for increasing values along *either* axis. That is, Auger recombination dominates in low injection and some cases of high injection. Radiative recombination, by contrast, affects V_{oc}—approximately as much as Auger—only in the lower left corner of the figure, which corresponds to high injection!

Finally, Figure 3(c) is a blend of Figures 3(a) and 3(b), with the V_{oc} lower than the lowest of the two V_{oc}s from those figures. With the chosen SRH parameters, SRH recombination dominates at low photogenerated current density, while intrinsic recombination dominates at high current density and at very high doping (Figure 4(c)). For a typical solar wafer and one-sun illumination, which is indicated by a yellow star, the V_{oc} is 725 mV and is nearly equally determined by intrinsic and SRH recombination. The cell is approaching high injection at open circuit ($\Delta n = 5n_0$).

Figures 5(a)–5(c) show contour plots of the exact *FF*s extracted from the same *J*–*V* curves used to create Figure 3. (Note that each column in Figure 5 has a different color scale because the range of *FF* values varies considerably depending on the recombination mechanism.) As is commonly observed experimentally, *FF* and V_{oc} are somewhat correlated (cf. Figures 3 and 5). However, the shape of the *FF* and V_{oc} contours are far from identical because, unlike V_{oc}, *FF* is approximately a *ratio* of voltages—the voltages at maximum power and open circuit. (This simplified statement in fact assumes that J_{mpp}/J_{sc} is constant. In fact, it varies from 0.9 to 0.97 across the contour plots—see Appendix B.) In addition, the *FF*s in the case of only intrinsic and only SRH recombination give us little insight into the *FF* when both mechanisms are present. Figure 5(c) looks more like Figure 5(b) than Fig. 5(a), but with considerably higher values. In particular instances, *FF* is additionally complicated by the fact that the dominant recombination mechanism can be, e.g., SRH at the maximum power point but Auger at open circuit. For a typical solar wafer under one-sun illumination—denoted again by a yellow star—the *FF* is 79%, which is nearly 10% lower than the intrinsic-recombination-limited *FF* and roughly equal to the SRH-limited *FF*. Interestingly, increasing *or* decreasing the photogenerated current density for this cell will result in a larger *FF*, even though the V_{oc} increases monotonically with current density. The cell is between low and mid injection at maximum power ($\Delta n = 0.3n_0$).

Using the exact V_{oc}s in Figure 3, we can now return to Equation (10) to find the associated approximate *FF*s and

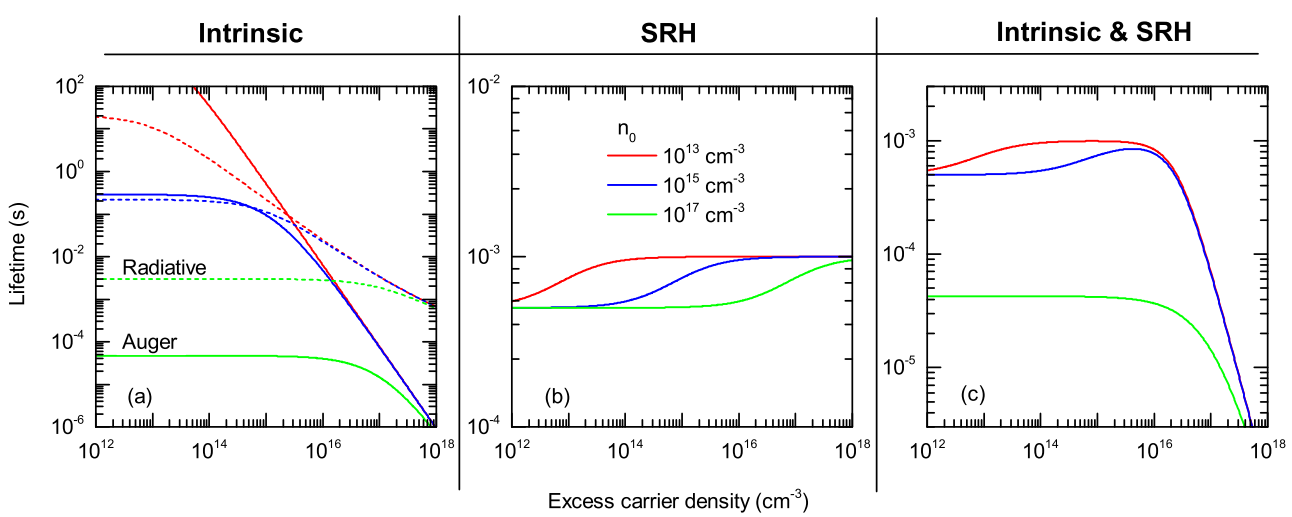

FIG. 4. Injection-dependent lifetime curves of silicon solar cells on n-type, 170-μm-thick wafers with varying doping density. Lifetimes are shown for cells with intrinsic recombination, SRH recombination, and intrinsic and SRH recombination in (a), (b), and (c), respectively.

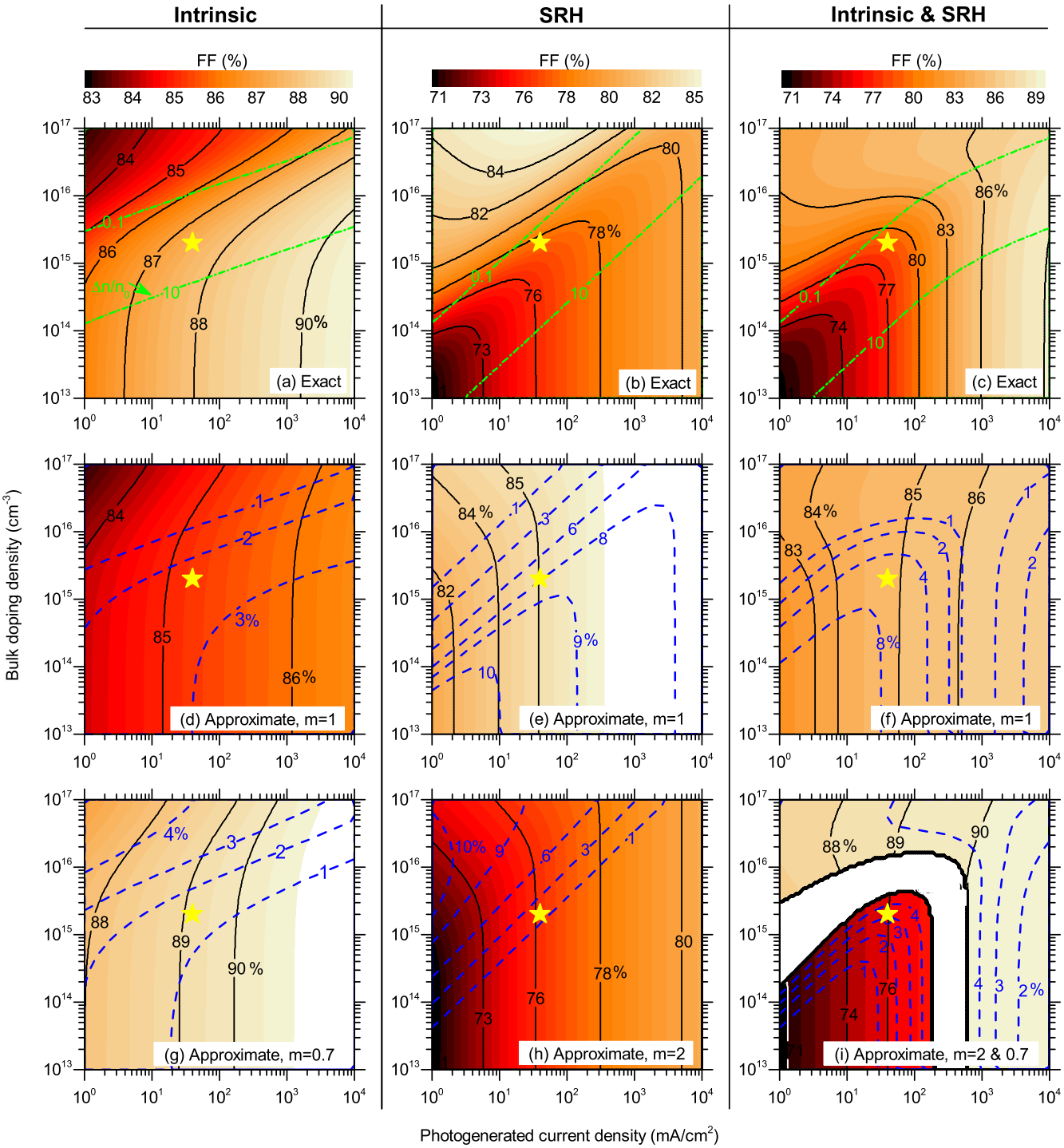

FIG. 5. ((a)–(c)) Exact and ((d)–(i)) approximate *FF*s of silicon solar cells on n-type, 170-μm-thick wafers with varying doping density under varying illumination levels (photogenerated current densities). *FF*s are shown for cells with intrinsic recombination, SRH recombination, and intrinsic and SRH recombination in the first, second, and third columns, respectively. The color scale is the same for each column, but not across columns. The dash-dotted green lines in ((a)–(c)) denote doping densities and photogenerated current densities for which n/n_0 is 0.1 or 10; these values are used to denote the boundaries of low injection (region above the upper green line) and high injection (region below the lower line). The yellow stars correspond to a typical solar cell with a 2 Ω cm n-type wafer under AM1.5G illumination. The approximate *FF*s in ((d)–(i)) were calculated using the V_{oc}s shown in Figure 3 and the assumed (constant) ideality factors shown. The blue dashed lines are contours of constant error in the *FF* in absolute percent.

compare them to the exact *FF*s in Figure 5. However, to use the expression, we also require an ideality factor. An ideality factor of $m = 1$ is most commonly assumed in the literature, and Figures 5(d)–5(f) show the resulting approximate *FF*. Note that the V_{oc}s in Figure 3(a) were used to generate Figure 5(d), the V_{oc}s in Figure 3(b) were used to generate Figure 5(e), and the V_{oc}s in Figure 3(c) were used to generate Figure 5(f). Comparing the colors in Figures 5(d)–5(f) to those in Figures 5(a)–5(c), there is little correlation between the exact *FF* and the approximate *FF* for any of the three recombination cases. The blue dashed lines are isocontours of the error in the *FF* in percent (absolute). Though the

inaccuracy is less than 1% in the upper left regions of Figures 5(d)–5(f), it reaches about 6% for a typical solar cell (yellow star) with both SRH and intrinsic recombination. That is, using the approximate expression with $m = 1$ for this cell predicts an overestimated FF of 85% when in fact the recombination limit is 79%.

What if, instead of assuming $m = 1$ under all conditions, we differentiate between low and high injection? The cutoffs for low and high injections are denoted by green dash-dotted lines in Figures 5(a)–5(c). According to the theory elaborated in Appendix A, intrinsic recombination has a constant ideality factor of $m = 1$ in low injection and a constant ideality factor of $m \approx 0.7$ in high injection (where it is dominated by Auger recombination). SRH recombination also has a constant ideality factor of $m = 1$ in low injection, but the ideality factor converges to $m = 2$ in high injection. We can now understand why the approximate FF in Figures 5(d)–5(f) is most accurate in the upper left corner of the plots: this area corresponds to low injection, for which $m = 1$, as was assumed. Figures 5(g)–5(i) plot the FF calculated with the approximate expression using the high-injection ideality factor for each recombination mechanism. The expression is again quite accurate in the injection range for which the ideality factor is appropriate (the lower right corner of the contour plots) for intrinsic recombination and SRH recombination. When the mechanisms are considered together in Figure 5(i), however, it is not clear which ideality factor to use, and using $m = 0.7$ and $m = 2$ in the areas where intrinsic and SRH recombination dominate, respectively, produces unsatisfying results. In particular, the FF of a typical solar cell is incorrect by 3.5% absolute.

Based on Figure 5, it appears that the approximate FF expression may be accurate if the correct ideality factor is used; the challenge is selecting that ideality factor. Each data point in Figures 3 and 5(a)–5(c) was extracted from an implied J–V curve generated from a simulated lifetime curve, and Equation (9) calculates the ideality factor from such lifetimes. We therefore have the luxury of knowing the ideality factor as a function of excess carrier density ($m(\Delta n)$) for every doping density and photogenerated current density. Which carrier density should we use when calculating the ideality factor for the approximate FF expression? Since the

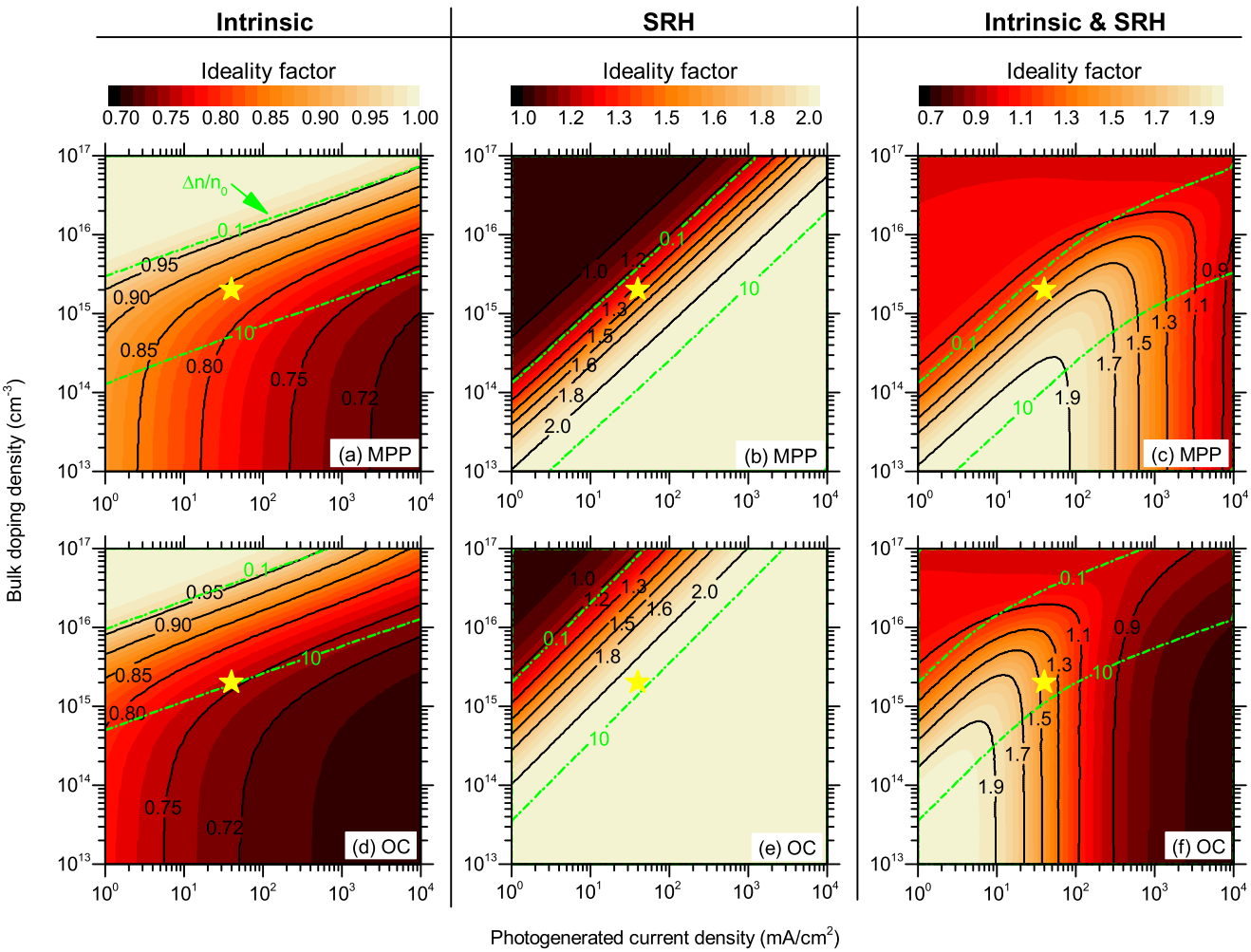

FIG. 6. Ideality factors at ((a)–(c)) maximum power and ((d)–(f)) open circuit of silicon solar cells on n-type, 170-μm-thick wafers with varying doping density under varying illumination levels (photogenerated current densities). Ideality factors are shown for cells with intrinsic recombination, SRH recombination, and intrinsic and SRH recombination in the first, second, and third columns, respectively. The color scale is the same for each column but not across columns. The dash-dotted green lines denote doping densities and photogenerated current densities for which n/n_0 is 0.1 or 10; these values are used to denote the boundaries of low injection (region above the upper green line) and high injection (region below the lower line). The yellow stars correspond to a typical solar cell with a 2 Ω cm n-type wafer under AM1.5G illumination.

expression gives *FF*, a natural choice is the carrier density corresponding to the maximum power point; the resulting ideality factor is plotted in Figures 6(a)–6(c). Another reasonable option is the ideality factor corresponding to open circuit since the expression takes V_{oc} as input; the ideality factor for this case is plotted in Figures 6(d)–6(f).

Note that in Figures 6(a) and 6(d), the ideality factor transitions from $m = 1$ to $m = 0.7$ when moving from low to high injection, as expected from Appendix A for intrinsic recombination. Similarly, it transitions from $m = 1$ to $m = 2$ in Figures 6(b) and 6(e), as expected for SRH recombination. Our typical solar cell has an ideality factor of $m = 1.4$ at both maximum power and open circuit, which is not like any of the ideality factors assumed in Figure 5.

Figures 7(a) and 7(b) depict the *FF* calculated with the approximate expression using the precise ideality factors corresponding to the excess carrier densities at maximum power and open circuit, respectively. That is, Figures 7(a) and 7(b) are like Figure 5(f) or Fig. 5(i), but instead of a constant ideality factor, the exact, injection-level-dependent ideality factors shown in Figures 6(c) and 6(f) were used. Note that both intrinsic and bulk defect recombination mechanisms were considered. Comparing the colors in Figures 7(a), 7(b), and 5(c) readily reveals that the approximate expression cannot replicate the exact *FF* in all cases even if the true ideality factor is known; there is an inherent problem in using a single ideality factor to calculate a quantity that depends on two injection levels. Nevertheless, the expression can come close in select instances, even for cells not in distinctly low or high injection: For our typical solar cell, the absolute error in the *FF* is 2.6% in Figure 7(a) and 1.7% in Figure 7(b). (As in Figure 5, the blue dashed lines are error isocontours.) However, even if somewhat accurate, this approach is impractical. One is unable to simply guess the best ideality factor to use, and the method employed here—plot a *J*–*V* curve from lifetime data, find the maximum power point or open circuit, determine the associated Δn, and use Equation (9) to calculate *m* at that Δn—yields the exact *FF* directly (from the *J*–*V* curve) in fewer steps.

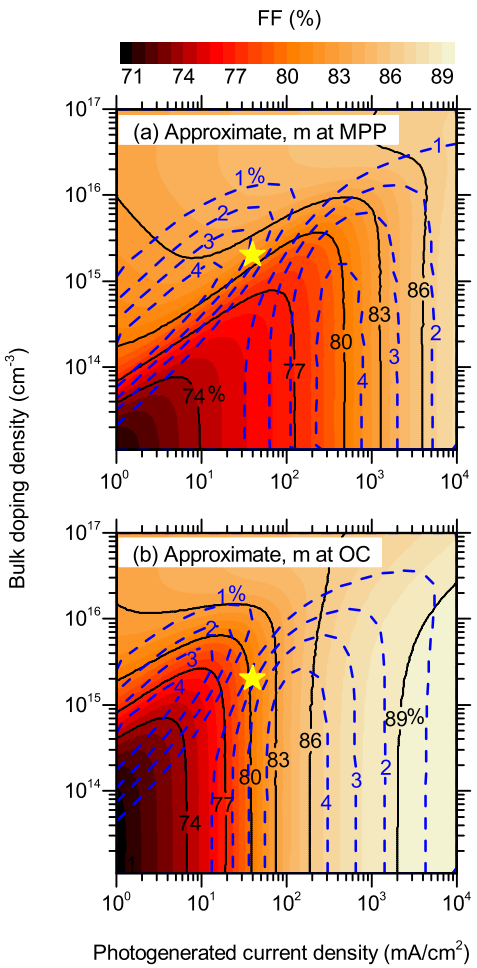

FIG. 7. Approximate *FF*s of silicon solar cells on n-type, 170-μm-thick wafers with varying doping density under varying illumination levels (photogenerated current densities). *FF*s are shown for cells with intrinsic and SRH recombination, and were calculated using the V_{oc}s shown in Figure 3 and the ideality factors at (a) maximum power or (b) open circuit (the ideality factors are shown in Figures 6(c) and 6(f)). The color scale is the same for both plots. The yellow stars correspond to a 2 Ω cm n-type wafer under AM1.5G illumination. The blue dashed lines are contours of constant error in the *FF* in absolute percent.

IV. CONCLUSION

We investigated the accuracy of the approximate expression proposed by Green for the recombination-limited *FF* of hypothetical silicon solar cells. Though accurate for low-defect-density solar cells in very high and very low injection if ideality factors of 0.7 and 1 are used, the formula gives unacceptable errors for today's cells in typical operating conditions. Furthermore, while we considered only intrinsic recombination and SRH recombination at a single defect, introducing surface recombination or multiple bulk defects in our analysis may exacerbate the error, particularly if the recombination mechanisms have strong injection dependence. One problem is that the "correct" ideality factor is unknown; a more insidious problem is that it *cannot* be known, as a single ideality factor is insufficient to predict *FF*. The root cause is that the *FF* is determined by the recombination at both the maximum power point and open circuit (and, to a lesser extent, short circuit). As the dependence of the recombination rate on the excess carrier density frequently changes between these two operating points—which is reflected in a changing ideality factor—no simple analytical expression can capture the complexity of *FF*. An extension of this conclusion is that, to accurately reflect the physics inside an operating cell, the ideality factor(s) in diode models should be a function of (implied) voltage.

What, then, are good practices for predicting the *FF* upper limit? We suggest calculating *iFF* from measured—or, if necessary, simulated—lifetime curves, as we have done here and others have done before.[4,19,35] This approach is becoming more common for silicon solar cells and has recently been codified in the newest quasi-steady-state photoconductance decay (QSSPC) software from Sinton Instruments. Most other cell technologies, however, are not amenable to QSSPC measurements and no other comparatively simple technique presently exists to generate lifetime data as a function of injection level. These technologies would greatly benefit from new measurement methods, as they would facilitate accurate analyses of *FF* losses and prevent misuse of approximate formulas like that from Green.

APPENDIX A: IDEALITY FACTORS IN LOW AND HIGH INJECTION

In order to calculate the ideality factor in both low and high injection for different recombination mechanisms, we rewrite Equation (7) as

$$(p_0 + \Delta n)(n_0 + \Delta n) = n_i^2 \exp\left(\frac{qV}{k_B T}\right). \tag{A1}$$

In low injection, Equation (A1) can be reorganized to give

$$\Delta n = \frac{n_i^2}{n_0} \exp\left(\frac{qV}{k_B T}\right). \tag{A2}$$

TABLE I. Lifetimes in low and high injection for individual recombination mechanisms.

	Auger	Radiative	SRH
Low injection	$\tau = \frac{1}{C_{Low,Aug} {n_0}^2}$	$\tau = \frac{1}{C_{Low,Rad} n_0}$	$\tau = C_{Low,SRH}$
High injection	$\tau = \frac{1}{C_{High,Aug} \Delta n^{1.92}}$	$\tau = \frac{1}{C_{High,Rad} \Delta n}$	$\tau = C_{High,SRH}$

In high injection, Equation (A1) instead becomes

$$\Delta n = n_i \exp\left(\frac{qV}{2k_B T}\right). \tag{A3}$$

TABLE II. Recombination current densities in low and high injection for individual recombination mechanisms.

	Auger	Radiative	SRH
Low injection	$J_{rec} = C_{Low,Aug} n_0 {n_i}^2 \exp\left(\frac{qV}{1k_B T}\right)$	$J_{rec} = C_{Low,Rad} {n_i}^2 \exp\left(\frac{qV}{1k_B T}\right)$	$J_{rec} = \frac{qW{n_i}^2}{n_0 C_{Low,SRH}} \exp\left(\frac{qV}{1k_B T}\right)$
High injection	$J_{rec} = C_{High,Aug} {n_i}^2 \exp\left(\frac{qV}{\frac{2}{2.92}k_B T}\right)$	$J_{rec} = C_{High,Rad} {n_i}^2 \exp\left(\frac{qV}{1k_B T}\right)$	$J_{rec} = \frac{qWn_i}{C_{High,SRH}} \exp\left(\frac{qV}{2k_B T}\right)$

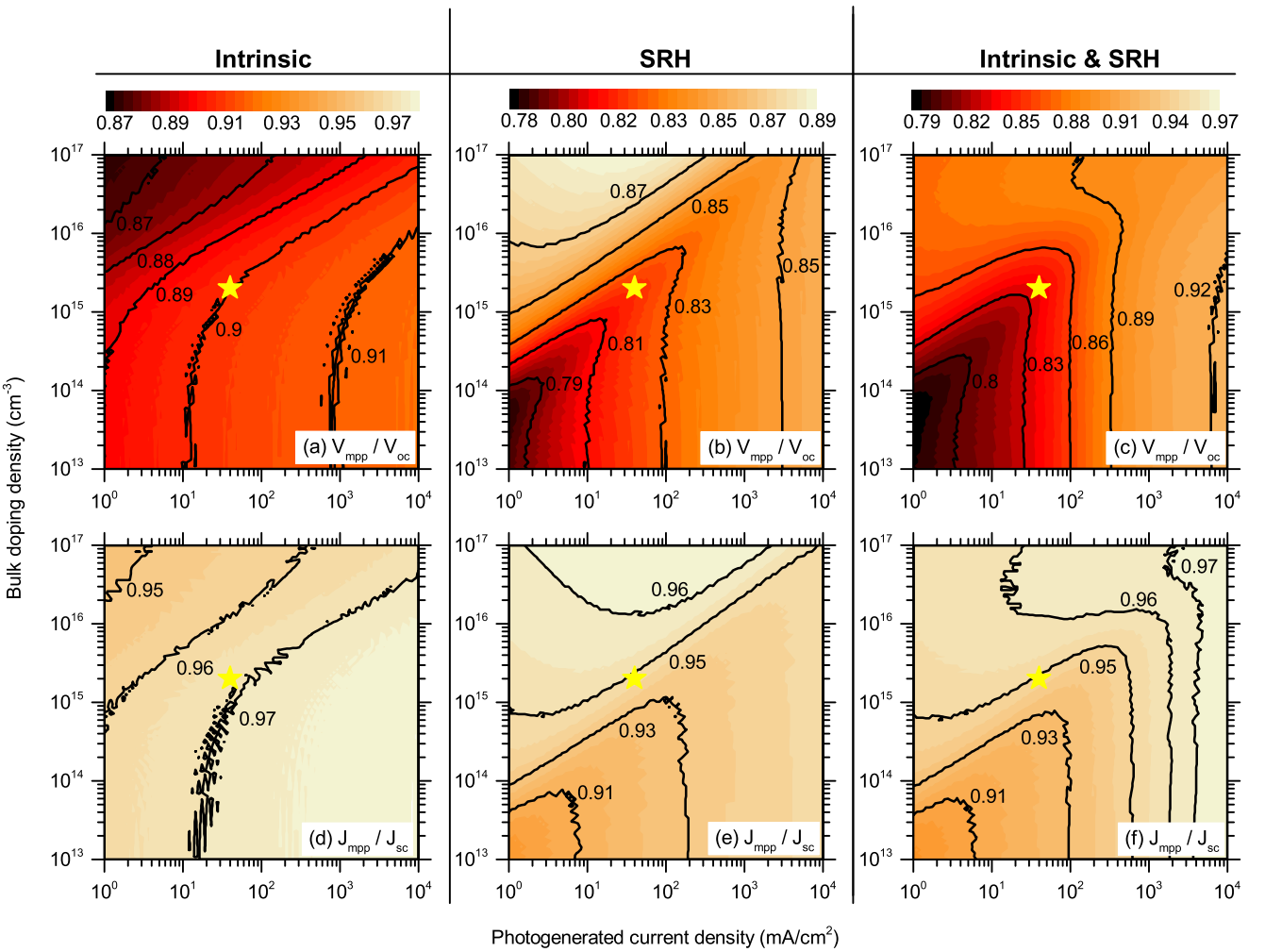

FIG. 8. ((a)–(c)) V_{mpp}/V_{oc} and ((d)–(f)) J_{mpp}/J_{sc} of silicon solar cells on n-type, 170-μm-thick wafers with varying doping density under varying illumination levels (photogenerated current densities). Ratios are shown for cells with intrinsic recombination, SRH recombination, and intrinsic and SRH recombination in the first, second, and third columns, respectively. The color scale is the same for each column, but not across columns. The yellow stars correspond to a typical solar cell with a 2 Ω cm n-type wafer under AM1.5G illumination. The noisy contours are the result of numerical calculation error that arises when taking ratios.

The Auger, radiative, and SRH lifetime expressions (see Equations (1) and (3)) can each also be simplified in these two regimes as shown in Table I. The C_i terms are constants. According to Equation (8), the recombination current density is

$$J_{rec} = qW\frac{\Delta n}{\tau_{eff}}. \tag{A4}$$

Inserting Equations (A2) and (A3), as well as the lifetime expressions in Table I, into Equation (A4) leads to the recombination current density expressions in Table II. The ideality factors appear before k_BT in each expression. Note that $2/2.92 \approx 0.7$, which is close, but not identical to the theoretical value of 2/3 for Auger recombination.[36]

APPENDIX B: VOLTAGE AND CURRENT CONTRIBUTIONS TO MAXIMUM POWER

For intrinsic recombination, SRH recombination, and the two together, Figure 8 shows the ratio of the voltages at maximum power and open circuit (V_{mpp}/V_{oc}; top row) and the ratio of the current densities at maximum power and short circuit (J_{mpp}/J_{sc}; bottom row). Their product is FF, which is shown in Figures 5(a)–5(c). This separation of FF into two components illustrates the relative importance of the voltage and current drops at maximum power, compared to open circuit and short circuit, respectively. The figure makes it clear that, though the contribution of J_{mpp}/J_{sc} to FF is not negligible (or constant for all conditions), V_{mpp}/V_{oc} always plays a more significant role.

[1]R. A. Sinton, A. Cuevas, and M. Stuckings, "Quasi-Steady-State Photoconductance, a New Method for Solar Cell Material and Device Characterization" in Proceedings of the IEEE 25th Photovoltaic Specialist Conferences (PVSC), Washington, 1996, p. 457.
[2]D. Pysch, A. Mette, and S. W. Glunz, Sol. Energy Mater. Sol. Cells **91**, 1698 (2007).
[3]M. A. Green, Solid-State Electron. **24**, 788 (1981).
[4]A. Descoeudres, Z. C. Holman, L. Barraud, S. Morel, S. De Wolf, and C. Ballif, IEEE J. Photovoltaics **3**, 83 (2013).
[5]Z. Hameiri, K. McIntosh, and G. Xu, Sol. Energy Mater. Sol. Cells **117**, 251 (2013).
[6]X. Guo, N. Zhou, S. J. Lou, J. Smith, D. B. Tice, J. W. Hennek, R. P. Ortiz, J. T. L. Navarrete, S. Li, and J. Strzalka, Nat. Photonics **7**, 825 (2013).
[7]Z. Fu, W. Shen, R. He, X. Liu, H. Sun, W. Yin, and M. Li, Phys. Chem. Chem. Phys. **17**, 2043 (2015).
[8]S. Yoo, B. Domercq, and B. Kippelen, J. Appl. Phys. **97**, 103706 (2005).
[9]Z. Huang, G. Natu, Z. Ji, M. He, M. Yu, and Y. Wu, J. Phys. Chem. C **116**, 26239 (2012).
[10]K. J. Singh and S. K. Sarkar, Opt. Quantum Electron. **43**, 1 (2012).
[11]Y. Wang, A. Gerger, A. Lochtefeld, L. Wang, C. Kerestes, R. Opila, and A. Barnett, Sol. Energy Mater. Sol. Cells **108**, 146 (2013).
[12]S. De Wolf, A. Descoeudres, Z. C. Holman, and C. Ballif, Green **2**, 7 (2012).
[13]D. Mbewe, H. Card, and D. Card, Sol. Energy **35**, 247 (1985).
[14]P. Loper, B. Niesen, S.-J. Moon, S. Martin de Nicolas, J. Holovsky, Z. Remes, M. Ledinsky, F.-J. Haug, J.-H. Yum, and S. De Wolf, IEEE J. Photovoltaics **4**, 1545 (2014).
[15]M. Diaz, L. Wang, D. Li, X. Zhao, B. Conrad, A. Soeriyadi, A. Gerger, A. Lochtefeld, C. Ebert, and R. Opila, Sol. Energy Mater. Sol. Cells **143**, 113 (2015).
[16]A. Richter, S. W. Glunz, F. Werner, J. Schmidt, and A. Cuevas, Phys. Rev. B **86**, 165202 (2012).
[17]W. Shockley and W. Read, Jr., Phys. Rev. **87**, 835 (1952).
[18]R. N. Hall, Phys. Rev. **87**, 387 (1952).
[19]A. Richter, M. Hermle, and S. W. Glunz, IEEE J. Photovoltaics **3**, 1184 (2013).
[20]T. Trupke, M. A. Green, P. Würfel, P. Altermatt, A. Wang, J. Zhao, and R. Corkish, J. Appl. Phys. **94**, 4930 (2003).
[21]P. Altermatt, F. Geelhaar, T. Trupke, X. Dai, A. Neisser, and E. Daub, Appl. Phys. Lett. **88**, 261901 (2006).
[22]A. Schenk, J. Appl. Phys. **84**, 3684 (1998).
[23]D. Yan and A. Cuevas, J. Appl. Phys. **114**, 044508 (2013).
[24]S. Rein, T. Rehrl, W. Warta, and S. Glunz, J. Appl. Phys. **91**, 2059 (2002).
[25]T. Tiedje, E. Yablonovitch, G. D. Cody, and B. G. Brooks, IEEE Trans. Electron Devices **31**, 711 (1984).
[26]M. A. Green, Prog. Photovoltaics **7**, 327 (1999).
[27]R. M. Swanson and R. A. Sinton, in *Advances in Solar Energy*, edited by K. A. Bouer (American Solar Energy Society, Newark, Delaware, 1990).
[28]K. W. Böer, *Advances in Solar Energy: An Annual Review of Research and Development* (Springer Science and Business Media, 2012), Vol. 6.
[29]K. Graff, *Metal Impurities in Silicon-Device Fabrication* (Springer Science and Business Media, 2013), Vol. 24.
[30]B. B. Paudyal, K. R. McIntosh, D. H. Macdonald, and G. Coletti, J. Appl. Phys. **107**, 054511 (2010).
[31]J. E. Birkholz, K. Bothe, D. Macdonald, and J. Schmidt, J. Appl. Phys. **97**, 103708 (2005).
[32]S. Rein and S. Glunz, J. Appl. Phys. **98**, 113711 (2005).
[33]J. Schmidt, R. Krain, K. Bothe, G. Pensl, and S. Beljakowa, J. Appl. Phys. **102**, 123701 (2007).
[34]Z. Xiong, Z. Zhang, H. Ye, S. Fu, P. Altermatt, Z. Feng, and P. Verlinden, "High performance multicrystalline wafers with lifetime of 400 μs at industrial scale," in Proceedings of the IEEE 42nd Photovoltaic Specialist Conference (PVSC), New Orleans, 2015.
[35]M. Reusch, M. Bivour, M. Hermle, and S. W. Glunz, Energy Proc. **38**, 297 (2013).
[36]M. J. Kerr, A. Cuevas, and P. Campbell, Prog. Photovoltaics: Res. Appl. **11**, 97 (2003).